Characterization and evaluation of arsenic and boron adsorption onto natural geologic materials, and their application in the disposal of excavated altered rock

Carlito Baltazar Tabelin[1]*, Toshifumi Igarashi[2], Takahiko Arima[3], Daiki Sato[4], Takeshi Tatsuhara[5] and Shuichi Tamoto[6]

[1]*Laboratory of Soil Environment Engineering, Faculty of Engineering, Hokkaido University, Sapporo 060-8628, JAPAN*
[2]*Laboratory of Groundwater and Mass Transport, Faculty of Engineering, Hokkaido University, Sapporo 060-8628, JAPAN*
[3]*Nippon Koei Co., Ltd., Tokyo 102-0083, JAPAN*
[4]*Shimizu Corporation, Tokyo 150-8007, JAPAN*
[5]*Pacific Consultants Co., Ltd., Tokyo 163-0730, JAPAN*
[6]*Civil Engineering Research Institute for Cold Region, Public Works Research Institute, Sapporo 062-8608, JAPAN*

E-mails: carlito@trans-er.eng.hokudai.ac.jp, a7139@n-koei.co.jp, daiki.sato@shimz.co.jp, takeshi.tatsuhara@tk.pacific.co.jp, 95353@ceri.go.jp and tosifumi@eng.hokudai.ac.jp

Abstract

Construction of tunnels in Hokkaido, Japan often excavates rocks containing substantial amounts of arsenic (As) and boron (B). When these rocks are exposed to the environment, As and B are leached out that could potentially contaminate the surrounding soil and groundwater. Natural geologic materials contain minerals like Al-/Fe- oxyhydroxides/oxides that have As and B adsorption capabilities. Because these materials are widespread and readily available, they could be utilized in the mitigation of As and B leached out from these sources. This paper describes the ability of three natural geologic materials (*i.e.*, pumiceous tuffs, partly-weathered volcanic ashes and coastal marine sediments) to sequester As and B from aqueous solutions and the actual leachate of an hydrothermally altered rock. The adsorption of As fitted well with either the Langmuir or Freundlich isotherm while those of B followed the Henry-type model (linear). Among the samples, those containing substantial amorphous Al and Fe exhibited higher As adsorption. However, the distribution coefficient of B only had a moderate positive correlation with these amorphous phases. The best adsorbent among these natural geologic materials was utilized in the adsorption layer of the column experiments. Adsorption of As was more effective the thicker the adsorption layer, but this retardation was only temporary due to significant changes in the pH. In contrast, the adsorption layer only retarded the migration of B to a limited extent.

Keywords: Arsenic, boron, adsorption, altered rocks, column experiments

*Corresponding author: Tel: +81-11-706-6311 Fax: +81-11-706-6308

email: carlito@trans-er.eng.hokudai.ac.jp

1 Introduction

Arsenic (As) and boron (B) are toxic at high concentrations and could cause a variety of human health and developmental problems. Chronic ingestion of trace amounts of As could cause arsenicosis, keratosis and cancers of the lungs, skin, bladder and kidneys (Chakraborty and Saha, 1987; Chen *et al.*, 1992). On the other hand, B is an essential micronutrient, but has been reported to cause reproductive and developmental abnormalities at large doses (Fail *et al.*, 1998). In nature, both of these elements are found only in trace amounts, but they are sometimes concentrated in certain geological features and anomalies. For instance, volcanic activities could cause hydrothermal alteration and the subsequent enrichment of rocks with As and heavy metals (Pirajno, 2009).

Hydrothermally altered rocks, which are abundant in Japan, are formed underground so that they usually do not pose any environmental problems. Unfortunately, recent tunnel projects for roads and railways have excavated these rocks exposing them to the environment. If not disposed of properly, sulfide minerals in the rocks are oxidized and weathered resulting in the release of hazardous elements into the surrounding soil and groundwater. At the moment, they are disposed of in landfills with special liners similar to those used for municipal solid and industrial wastes (Katsumi *et al.*, 2001; Lundgren and Soderblom, 1985; Wijeyesekera *et al.*, 2001). However, this approach on the long term is not economically sustainable because of its prohibitively high cost in conjunction with the large volume of rocks excavated. In search of an alternative mitigation approach, we have studied in detail the leaching behavior and release mechanisms of several hazardous elements present in altered rocks (Tabelin and Igarashi, 2009). We have also found that altered rocks could partly mitigate the leaching of As through its adsorption onto

precipitated iron (Fe)- and aluminum (Al)-oxides/oxyhydroxides (Tabelin *et al.*, 2012b). However, the adsorption capabilities of these inherent minerals were insufficient to lower the concentration of As below the environmental standard of Japan (10 μg/L) (Tabelin *et al.*, 2012b,c). Based on these previous results, a viable countermeasure to mitigate the leaching of As is to enhance the sequestration capability of altered rocks through the addition of suitable adsorbents.

Mohan and Pittman (2007) provided a comprehensive review of As adsorbents used in water and wastewater treatments. However, most of these studies pertain to either synthetic materials/minerals or naturally occurring materials that are composed of only a single mineral (*e.g.*, natural hematite, bentonite and kaolinite).Thus, studies pertaining to the adsorption of As and B onto naturally occurring materials with complex mineral compositions are still lacking. Likewise, adsorption of As and B onto single component/mineral systems could not be used to predict the transport of these elements in multi-component systems like rocks and soils.

In this study, we evaluated As and B adsorption onto pumiceous tuff, partly-weathered volcanic ash and coastal sediments using classical batch adsorption experiments. Because most of these samples have trace amounts of As, the leachability of this geogenic As as a function of pH was also elucidated in selected samples. The best adsorbent was selected based on the leaching and adsorption results, and used to mitigate the leaching of As and B from an actual hydrothermally altered rock. This was done using column experiments with a crushed rock-bottom adsorption layer configuration (Tatsuhara *et al.*, 2012), which is similar to the concept of permeable reactive barriers (PRB). Finally, the migration of As and B was simulated using the one-dimensional advection-dispersion with retardation equation to provide insights into the transport phenomena in the adsorption layer.

2 Materials and methods

2.1 Sample collection, preparation and characterization

The hydrothermally altered rock sample was collected from a road tunnel built in the central part of Hokkaido, Japan. The rock excavated in this area is mainly composed of partly altered mudstone and sandstone of marine origin from the Cretaceous period. The rock sample was collected from an interim storage site, which was built to accommodate freshly excavated rocks from the tunnel prior to their final disposal. Thus, the rocks have been partly oxidized due to its exposure to the environment for ca. 6 months. Sampling was done using shovels at random points around the interim storage site with collected samples varying in sizes from gravel (> 20 mm in diameter) to silty sand (< 2mm in diameter). The rock sample was brought to the laboratory, air dried at room temperature, crushed using a jaw crusher and sieved through a 2 mm aperture screen. The < 2 mm fraction was collected, mixed thoroughly and stored in air-tight containers to minimize its exposure to moisture. During the tunnel construction, the rocks excavated usually have a wide distribution of sizes ranging from large boulders to very fine silt and clay. We chose to evaluate the < 2 mm fraction because it represented the most reactive fraction of the bulk excavated rock. The chemical composition and mineralogical properties of this rock has been reported previously (Tabelin *et al.*, 2012a, 2012d). It is composed predominantly of silicate minerals (*i.e.*, quartz and plagioclase), chlorite and calcite as minor minerals, and trace amount of pyrite. It contains As and B at 6.9 and 113 mg/kg, respectively. In terms of the particle size distribution of the altered rock sample used in the column experiments, it is classified as loamy sand, which is composed of 89.4% sand, 5.3% fine sand, and 5.3% silt and clay.

Eleven natural geologic materials were collected for the experiments: three pumiceous tuffs (T-1, 2 and 3), two partly-weathered volcanic ashes (A-1 and A-2) and six coastal sediments (S-1 – 6). The three pumiceous tuffs and one volcanic ash (T-1 – 3; A-1) originated from the previous eruptions of Mt. Tokachi located around Obihiro City (central part of Hokkaido). The other volcanic ash sample (A-2) came from the town of Kucchan (western part of Hokkaido) while all six coastal sediments were obtained near Hakodate City (southern part of Hokkaido). A brief description of these materials is summarized in Table 1. Samples of these geologic materials in their undisturbed state were collected using stainless steel cylinders for the determination of their hydraulic conductivities. Additional samples were obtained using hand shovels, air dried at room temperature, lightly crushed using mortar and pestle and sieved through a 2 mm aperture screen. The < 2 mm fraction was utilized in the adsorption, leaching and column experiments. Chemical and mineralogical analyses were carried out on pressed powders of the samples (< 50 μm) using an X-ray fluorescence spectrometer (Spectro Xepos, Rigaku Corporation, Japan) and an X-ray diffractometer (MultiFlex, Rigaku Corporation, Japan), respectively. Other important properties of these materials like particle size distribution and particle density were also measured. Their amorphous Al and Fe contents were determined by acidic oxalate solution extraction (McKeague and Day, 1965; Tamm, 1922), which was done by mixing 1 g of sample and 100 ml of acidic oxalate solution for 4 hours at room temperature. The acidic oxalate solution was a 1:0.75 mixture of 0.23 M ammonium oxalate ($C_2H_8N_2O_4$) and 0.28 M oxalic acid ($H_2C_2O_4$). Zeta potential of the adsorbent used in the column experiments was measured using Nano-ZS60 (Malvern Instruments, UK). This analysis was done on the < 50 μm fraction using 0.1 M hydrochloric acid (HCl) or sodium hydroxide (NaOH) solution for pH adjustment.

2.2 Batch experiments

2.2.1 pH dependent leaching experiments

Batch leaching experiments were conducted under ambient conditions by mixing 15 g of selected natural geologic samples (< 2 mm) and 150 ml of prepared leachants. HCl and NaOH solutions of varying concentrations were used as leachants. The deionized water (18MΩ·cm) used during the leachant preparation was obtained from a Millipore Milli-Rx 12α system (Merck Millipore, USA). After 24 hours, the pH and redox potential (Eh) of the suspensions were measured followed by filtration of these suspensions through 0.45 μm Millex® sterile membrane filters (Merck Millipore, USA). All filtrates were acidified (pH < 2) and stored at 6°C prior to the chemical analyses.

2.2.2 Arsenic and boron adsorption experiments

Batch adsorption experiments were done by mixing solutions of known arsenate (As[V]) or B concentration with various amounts of the natural geologic samples at 120 rpm for 24 hours. We only evaluated the adsorption of As[V] onto these natural materials because majority of As leached from the hydrothermally altered rock used in this study was As[V] (Igarashi *et al.*, 2013). As[V] was prepared from reagent grade $Na_2HAsO_4{\cdot}7H_2O$ powder while B was prepared from 1,000 mg/L standard solutions for atomic absorption spectrometry (Wako Pure Chemical Industries Ltd., Japan). The leachate samples were collected by filtration through 0.45 μm Millex® filters and analyzed for As and B. Solute concentration (*i.e.*, As or B) retained in the adsorbents was calculated using the following equation:

$$q = \frac{(C_o - C)\cdot V}{W} \qquad (1)$$

where, q is the adsorbed amount (mg/g), C_o is the initial solute concentration (mg/L), C is the final solute concentration (mg/L), V is the volume of solution (L), and W is the adsorbent weight (g).

Data from these experiments were fitted with the Henry-type (linear), Freundlich and Langmuir isotherms, which were calculated using equations (2), (3) and (4), respectively.

$$q = K_D \cdot C \quad (2)$$

$$q = K_f \cdot C^n \quad (3)$$

$$q = \frac{q_{max} \cdot L \cdot C}{1 + L \cdot C} \quad (4)$$

where, K_D in equation (2) is the distribution coefficient (L/g), K_f and n in equation (3) are empirical constants, and L and q_{max} in equation (4) correspond to the affinity of the adsorbent for the solute of interest (*i.e.,* As and B) and the maximum adsorption capacity of the solid (mg/g), respectively.

2.3 Column experiments

2.3.1 Apparatus and initial conditions

The columns were made from PVC tubes, which are mounted on top of a steel stand. The steel stand was configured to accommodate three columns. The PVC tubes have inner diameters of 105 mm and heights of 600 mm. Acrylic covers with small perforated holes were designed and placed on top of the columns to simulate rainfall. In the construction of the rock-adsorption layer column configuration, a pre-determined amount of the selected natural adsorbent was first put into the columns and compacted to a thickness corresponding to a bulk density of 0.72 g/cm^3. The hydrothermally altered rock was then placed on top of the adsorption layer and compacted to a bulk density of 1.28 g/cm^3. One column was constructed with the crushed rock only while the

other two were built with both rock and adsorption layers (10 and 30 mm thickness). The weight of rock and the thickness of the rock bed used in the three columns were the same. Details of the column experimental conditions and a schematic diagram of the column setup are summarized in Table 2 and Figure 1, respectively.

2.3.2 Irrigation and effluent collection

Deionized water was introduced once a week on top of each column via the rainfall simulator at amounts equivalent to 34.5 mm/week of rainfall, which is the average weekly rainfall in Japan, and allowed to flow by gravity. Polypropylene bottles were placed at the bottom of each column to collect the effluents. Because the columns were initially dry, the first effluents were collected ca. 4 weeks after the first irrigation. After this, effluents were regularly collected at the bottom of each column ca. 2 days after irrigation. This intermittent irrigation scheme means that the columns were under unsaturated flow conditions with a free drainage lower boundary condition. The pH, Eh and electrical conductivity (EC) of the effluents were measured, followed by filtration of the liquid samples through 0.45 μm Millex® filters. The filtrates were then acidified and stored at 6°C prior to the chemical analyses.

2.4 Chemical Analyses of liquid samples

Dissolved concentrations of As, B and coexisting ions like Si, Fe and Al greater than 0.1 mg/L were determined using an inductively-coupled plasma atomic emission spectrometer (ICP-AES) (ICPE-9000, Shimadzu Corporation, Japan). The leachates/effluents with As concentrations less than 0.1 mg/L were pre-treated and analyzed using a hydride vapor generator attached to the ICP-AES (Tabelin *et al.*, 2012b). Concentrations of B and coexisting ions less than 0.1 mg/L were analyzed using an ultrasonic aerosol generator attached to the ICP-AES. Cations like Ca^{2+}

and Na^+ were quantified using an ion chromatograph, ICS – 90 (Dionex Corporation, USA). Anions like SO_4^{2-} were also measured using ion chromatography (ICS – 1000, Dionex Corporation, USA). Bicarbonate (HCO_3^-) concentrations were calculated from the alkalinity, which was determined by titrating a known volume of the leachate/effluent with 0.02 N sulfuric acid (H_2SO_4) solution until pH 4.8. The standard ICP-AES method has a margin of error of ca. 2 – 3% while analyses using more sensitive hydride vapor and ultrasonic aerosol generators have uncertainties of ca. 5%.

3 Modelling of arsenic and boron migration

The migration of As and B through the adsorption layer was modeled using the one-dimensional advection-dispersion with retardation equation described below:

$$D_x \frac{\partial^2 C}{\partial x^2} - \bar{v} \frac{\partial C}{\partial x} - \frac{\rho_b}{\theta} \frac{\partial S}{\partial t} = \frac{\partial C}{\partial t} \qquad (5)$$

where, D_x is the longitudinal coefficient of hydrodynamic dispersion, C is the solute concentration, S is the mass of the chemical constituent adsorbed per unit mass of the solid phase of the porous medium, $\bar{v}$ is the average pore water velocity, x is the depth, ρ_b is the bulk density, θ is the volumetric water content and t is time. When solute adsorption is described by the linear isotherm (equation (2)), the distribution coefficient (K_D) is given by the equation below:

$$\frac{\partial S}{\partial C} = K_D \qquad (6)$$

An analytical solution to equation (5) is obtained when the input is a step function and adsorption is described by the linear isotherm. The initial and boundary conditions are described as follows:

$$C(x,0) = 0 \qquad x \geq 0$$

$$C(0,t) = C_o \qquad t \geq 0$$

$$C(\infty,0) = 0 \qquad t \geq 0$$

Under these conditions, the solution to equation (5) for a homogeneous medium was calculated by Ogata and Banks (1970) and described by the following equation:

$$\frac{C\,(x,t)}{C_o} = \frac{1}{2}\left\{erfc\left(\frac{R_f x - \bar{v}t}{2\sqrt{R_f D_x t}}\right) + exp\left(\frac{\bar{v}x}{D_x}\right) erfc\left(\frac{R_f x + \bar{v}x}{2\sqrt{R_f D_x t}}\right)\right\} \quad (7)$$

$$R_f = 1 + \frac{(1-n)\rho_b}{\theta} K_D \quad (8)$$

where, *erfc* is the complementary error function, and R_f is the retardation factor.

In case of a continuous source and assuming that time is finite; equation (7) can be transformed to equation (9).

$$\frac{C\,(x,t)}{C_o} = \frac{1}{2}\left\{erfc\left(\frac{R_f x - \bar{v}t}{2\sqrt{R_f D_x t}}\right) + exp\left(\frac{\bar{v}x}{D_x}\right) erfc\left(\frac{R_f x + \bar{v}x}{2\sqrt{R_f D_x t}}\right)\right\} - \frac{1}{2}\left\{erfc\left(\frac{R_f x - \bar{v}(t-t^*)}{2\sqrt{R_f D_x (t-t^*)}}\right) + exp\left(\frac{\bar{v}x}{D_x}\right) erfc\left(\frac{R_f x + \bar{v}x}{2\sqrt{R_f D_x (t-t^*)}}\right)\right\} \quad (9)$$

where, t^* is the time when the concentration becomes zero. The concentration change in the adsorption layer was calculated using the principle of superposition (*i.e.*, convolution of equation (9)). The average value of θ used in the analytical model was estimated from the water balances of the columns. Using Hydrus 1D (Jacques *et al.*, 2008; Šimůnek *et al.*, 2008) and parameters similar to our column experiments, we modelled solute migration under unsteady and steady state conditions. The analytical and numerical modelling results agreed fairly well with each

other so the assumption of pseudo-steady state flow in the analytical model is justified. Details of the parameters used in the analytical model including initial and boundary conditions are summarized in Table 3.

4 Results

4.1 Properties of the natural geologic materials

The physical and hydrological properties of the natural geologic materials are summarized in Table 4. T- and S-series samples were predominantly composed of sand- and silt-sized particles (>79%) while A-2 contained higher amounts of finer clay-sized particles. Regardless of these variations, the hydraulic conductivities of these samples were in the range classified as semi-permeable (10^{-5} – 10^{-6} m/s) that is ideal as bottom adsorption layer material.

The chemical and mineralogical compositions of these geologic materials are listed in Tables 5 and 6, respectively. Among the samples, A-1, A-2, S-1 and S-6 contained high amounts of Fe at 10.5, 9, 10.3 and 10.6 wt.% as Fe_2O_3, respectively. These four samples also contained substantial amounts of Al ranging from 17.1 – 24.0 wt.% as Al_2O_3. Most of these materials had very low S contents except A-2, and all of them contained trace amounts of As. S-5 had the highest As content at 8.1 mg/kg while A-1 had the least at 1.2 mg/kg. These natural materials were mainly composed of silicate minerals like quartz, albite, anorthite, muscovite and chlorite, but common Fe-bearing minerals like goethite (FeOOH) and hematite (Fe_2O_3) were not detected by the XRD analysis even though Fe contents were quite substantial. Moreover, only A-1, A-2 and S-1 had amorphous Fe and Al greater than 1 mmol/g (Table 7).

4.2 Leaching and adsorption properties of the natural geologic materials

The pH of most of the natural geologic materials when in contact with deionized water was slightly acidic (pH 6), and the leaching concentrations of As were insignificant (<0.1 µg/L). However, alkaline and strongly acidic conditions enhanced the leaching of geogenic As as illustrated in Figure 2. At pH <1, the concentration of As in the leachates of A-2 reached 19 µg/L. Similarly, substantial As leaching was observed in the hyper-alkaline pH range (pH>10) reaching 112 µg/L at pH 12 in A-1. The enhanced leaching of As from these samples simultaneously occurred with increases in the leachate concentrations of Fe and Al as shown in Figure 3. For A-2, concentrations of Fe and Al in the acidic pH reached more than 300 and 1,700 mg/L, respectively. Similarly, Fe and Al concentrations above pH 11 in A-1 increased to values higher than 2 and 60 mg/L, respectively.

Although all samples were evaluated, only four showed substantial adsorption affinities for As and B as illustrated in Figures 4 and 5, respectively. Constants of the linear, Freundlich and Langmuir isotherms are also summarized in Tables 8 and 9 for As and B, respectively. The samples with substantial As adsorption capabilities were A-1, A-2, S-1 and S-5 with maximum adsorption capacities (q_{max}) estimated at ca. 3, 2, 1.5 and 0.25 mg As/g adsorbent, respectively. On the other hand, the adsorption of B closely resembled linear isotherms. K_D values of A-2 and S-1 were higher than those of A-1 and S-5, indicating that A-2 had the highest B adsorption among all the samples. However, these materials sequestered 2 – 3 orders of magnitude more As than B. Arsenic adsorption was also strongly correlated with the amorphous Al and Fe contents of the samples (Figure 6). On the other hand, K_D values of B and the amorphous Al and Fe contents of the samples were moderately correlated.

Among the samples evaluated, A-1 had the lowest As content and best adsorption properties for As. Thus, it was selected as the natural adsorbent for the column experiments. Sample A-1 had a strong positively-charged surface from pH 2 – 5.5 (+18 – +25 mV) (Figure 7). Above pH 5.5, these positively charged surfaces diminished slowly until the isoelectric point (IEP) or point of zero charge (pH 7.1). Increasing the pH further resulted in the formation of negatively-charged surfaces.

4.3 Breakthrough curves of pH, Eh, EC, As, B and coexisting ions

The changes in pH, Eh and EC of the effluent with time in all cases are illustrated in Figures 8(a), (b) and (c), respectively. The initial effluent pH in case R (altered rock only) was slightly alkaline at 8.1, which increased with time and stabilized in the range of 10.1 – 11.5. The presence of adsorption layers lowered the initial leachate pH substantially. In case R+A1 (with 10 mm adsorption layer), the pH values were ca. two pH units lower between weeks 5 and 10 compared to case R. However, starting from ca. week 11, the pH gradually increased and approached those of case R. After week 15, the leachate pH in cases R and R+A1 were similar. Increasing the adsorption layer thickness to 30 mm (case R+A2) further decreased the effluent pH by an additional 1 – 2 pH units, and although the pH values approached those of case R, the increase was more gradual than in case R+A1. The Eh of the effluents increased in cases with adsorption layers. Similar to pH, the Eh values in case R+A1 approached those of case R while those of case R+A2 were ca. 100 mV higher until the end of the experiment. Regardless of these differences, the Eh values in all cases were greater than +150 mV, which indicates slightly – moderately oxidizing conditions. The EC curves had flushing out trends, that is, initially high EC values rapidly decreased with time followed by stabilization. However, EC values in cases R+A1

and R+A2 were considerably lower than that of case R, which indicates that the adsorption layer retarded the movement of dissolved ions.

Figures 8(d) – 8(h) show the breakthrough curves of As, B and major coexisting ions like Ca^{2+}, Na^{+} and SO_4^{2-}. In case R, an As concentration peak that reached ca. 100 µg/L was observed between weeks 3 and 7 (Figure 8(d)). After this peak, As concentration in the effluent rapidly decreased with time and stabilized after week 9 in the range of 48 – 62 µg/L. In case R+A1, As concentration began to increase above 10 µg/L after week 5. A thicker adsorption layer (case R+A2) further delayed this As concentration increase by more than 20 weeks. After this initial retardation, As concentration in case R+A2 gradually increased in both cases reaching levels similar to those of case R. B concentration in case R increased with time until a peak was reached, followed by gradual decrease until the end of the experiment (Figure 8(e)). The same trend was also observed in the cases with adsorption layers, but there was a clear decrease and delay in the B concentration peak. The B concentration peaks in cases R+A1 and R+A2 decreased by ca. 2 and 3 mg/L, respectively. Similarly, the 10 and 30 mm thick adsorption layers delayed the concentration peaks of B by ca. 2 and 3 weeks, respectively. The major cations of the column effluents were Ca^{2+} and Na^{+} while the major anion was SO_4^{2-}. These major ions (*i.e.*, Ca^{2+}, Na^{+} and SO_4^{2-}) had flushing-out trends similar to that of the EC, which indicates that these ions are present in the altered rock as soluble phases (Figures 8(c), (f), (g) and (h)).

Based on the mass balance calculations of As and B until week 32, the rock released 0.487 mg of As (case R), which is ca. 2% of the total As content of the sample. The total amount of As released from case R+A1 (0.614 mg) was higher than that of case R (0.487 mg), suggesting that substantial amount of As was released from the adsorption layer. Case R+A2 had the lowest amount of As released at 0.121 mg, which means that the adsorption layer retained 0.366 mg of

As corresponding to ca. 75% of the total amount of As released from the rock. For B, the altered rock released 65.6 mg, which is equivalent to 17.5% of the total B content of the rock. The amounts of B retained in the 10 and 30 mm adsorption layers were quite low at 14% (9.5 mg) and 12% (8.1 mg) of the total B leached from the rock, respectively.

4.4 Reactive transport modelling of As and B migration using the advection-dispersion with retardation equation

The migration of As and B was simulated using equation (9), and K_D values were fitted to the observed results of case R+A2 as illustrated in Figure 9. The results of case R+A2 were selected because the effect of As leaching from the adsorption layer was apparent in case R+A1. The model-calculated K_D values are found in the range of 10 – 50 and 3 – 10 ml/g for As and B, respectively. The analytical model was successfully fitted with the experimental results of B, but could not accurately predict the migration of As in the adsorption layer. The predicted K_D values for B were similar to that obtained from the batch adsorption experiments, indicating that the linear isotherm and advection-dispersion equation could be used to evaluate B migration in an altered rock-adsorption layer column setup. In contrast, the poor fit of the analytical model in the case of As suggests that its retardation in the adsorption layer could not be expressed in terms of K_D consistent with the results of the batch adsorption experiments.

5 Discussion

5.1 Potential of natural geologic materials as adsorbents of arsenic and boron

Natural geologic materials generally have geogenic As close to background levels. In this study, most of the samples have low geogenic As, but some of them have As higher than the rock that

needs mitigation (*e.g.*, S-1 and S-5). The geogenic As of these materials was quite stable especially between pH 2 and 10. Outside this pH range, however, significant amounts of As were mobilized. Under strongly acidic conditions, increased mobility of As could be attributed to the acid dissolution of Al- and Fe-bearing minerals like hydroxides/oxyhydroxides. This deduction is supported by the high concentrations of Al and Fe in the leachate under strongly acidic conditions (Figure 3). In the hyper-alkaline pH range, the release of As from these materials could be attributed to the combined effects of desorption and dissolution as indicated by the strongly negative zeta potential as well as the high concentrations of Fe and Al in the leachate (Figures 2, 3 and 7).

Some of the natural geologic materials evaluated in this study showed strong adsorption affinities for As. Their adsorption capacity increased proportional to their amorphous Fe and Al contents, which could be attributed to the net positively charged surfaces at pH 6 contributed by these phases as well as the strong adsorption affinity of As onto Fe- and Al-hydroxides/oxyhydroxides (Chen *et al.*, 2006; Dzombak and Morel, 1990; Manaka, 2006). Adsorption of As onto these samples fitted well with either the Freundlich or Langmuir isotherm, indicating that adsorption decreases at higher As loadings because of the progressive saturation of adsorption sites (Bethke, 2007). In other words, these materials could only adsorb a finite amount of As, and are best suited in systems with relatively low As concentrations (µg/L levels) such as leachates from altered rocks. Although B adsorption conformed well to the linear isotherm, its adsorption onto natural geologic materials was quite limited. This could be attributed to the low adsorption affinity of B onto these materials as well as the more conservative leaching behaviour of B compared to As (Tabelin *et al.*, 2012d).

5.2 Adsorption onto volcanic ash of arsenic and boron leached from altered rocks

Partly-weathered volcanic ash used in the adsorption layer temporarily retarded the mobilization of As because of two interrelated processes. First, volcanic ash, which has a pH of ca. 6 when in contact with water, acted as a buffer that lowered the leachate pH from alkaline to around circumneutral. Second, the As adsorption capability of the natural adsorbent was enhanced through the formation of more positively charged surfaces in this lower pH range. The Eh of the system is also an important factor in the mobility of As. Reducing conditions (*i.e.*, negative Eh values) enhance As leaching mainly through the reductive dissolution of Fe-oxyhydroxides, which act as As adsorbents, and the reduction of arsenate (As[V]) to more mobile arsenite species (As[III]) (Masscheleyn *et al.*, 1991; Mitsunobu *et al.*, 2006; Nickson *et al.*, 2000). This Eh-dependent leaching behaviour of As is usually observed in organic matter-rich systems where redox conditions change rapidly from oxic to anoxic and vice versa as a result of fluctuations in the water table level (*e.g.*, estuarine and riverine floodplain soils and sediments) (Du Laing *et al.*, 2009; Frohne *et al.*, 2011). In such systems, anoxic conditions coupled with organic matter driven microbial activities could considerably lower the Eh, resulting in the enhanced mobility of As. In this study, redox conditions were oxidizing as indicated by the measured Eh values of the leachates and effluents. Moreover, the altered rock and volcanic ash did not contain substantial amounts of organic matter that can fuel extensive microbial activities. Thus, the influence of pH on the mobility of As in our system is more prominent than that of Eh.

The effectiveness of the ash sample to sequester As dramatically decreased in the column experiments. There are three probable explanations for this phenomenon: (1) exhaustion/depletion of adsorption sites, (2) desorption due to alkaline pH, and (3) competition with other anions. Calculations using q_{max} and the total mass of ash in the adsorption layer

indicate that the adsorbent in cases R+A1 and R+A2 could ideally sequester ca. 62 and 187 mg of As, respectively. The total amount of As leached from the altered rock was less than 1 mg, indicating that adsorption sites were far from being depleted. This means that exhaustion of adsorption sites is not a viable explanation for the observed results. The altered rock persistently released alkaline leachates that ultimately depleted the buffering capability of the adsorbent, and raised the pH around 10 – 11. Because of this, the surface charges of Al- and Fe- oxyhydroxide phases became more negative minimizing adsorption and at the same time enhancing desorption of the As load of the ash layer. Increasing the thickness of the adsorbent layer three-fold retarded the migration of As longer, but signs of As desorption due to the alkaline pH (*i.e.*, higher As leaching concentrations compared to case R) were already apparent in case R+A2 towards the end of the experiment (Figure 8(d)). Coexisting ions known to compete with As for adsorption sites like Si and HCO_3^- also contributed to the reduced efficiency of the ash layer (Anawar *et al.*, 2004; Meng *et al.*, 2000). For instance, Meng *et al.* (2000) illustrated that small amounts of H_4SiO_4 (0 – 1 mg/L as Si) had negligible negative effects on As adsorption, but 10 mg/L of H_4SiO_4 decreased the amount of As adsorbed onto Fe-oxyhydroxides by ca. 50%. Starting from the fifth week until the end of the experiment, HCO_3^- and Si concentrations originating from the altered rock were relatively high (HCO_3^-: 280 – 336 mg/l; Si: 31 – 51 mg/l), which could have partly contributed to the lower As adsorption in the ash layer.

For B, the breakthrough curves were clearly independent of the pH consistent with our previous results (Tabelin *et al.*, 2012d). The adsorption layer also retarded the movement of B, but only to a limited extent regardless of its thickness. This means that adsorption of B onto natural geologic materials is not a viable mitigation approach in B-contaminated systems. Other authors have also pointed out the difficulty of B immobilization through adsorption. Perkins

(1995) reported that very little B is adsorbed onto slightly acidic soils (pH 4 – 5) and most of it would pass into solution as boric acid. Other materials like activated carbon and clays used for the removal of B in contaminated systems were also ineffective mainly because of the relatively slow adsorption kinetics of B (Xu and Jiang, 2008).

6 Conclusions

Several cheap and readily available natural geologic materials like pumiceous tuffs, partly-weathered volcanic ashes and coastal marine sediments were evaluated for their As and B adsorption capabilities. Some of these natural materials were fairly good adsorbents of As. Moreover, the As and B adsorption capabilities of these materials were strongly correlated with their amorphous Fe and Al contents, indicating that the concentration of amorphous Fe and Al in natural geologic materials could be used as a simple indicator of their effectiveness during the selection process. However, their applicability in the mitigation of As and B leached from hydrothermally altered rocks was fairly limited. Most of these natural materials contained geogenic As in trace amounts that could be mobilized under strongly acidic and alkaline conditions because of the dissolution of Fe- and Al-bearing minerals and desorption. In addition, all of them had very low adsorption affinities for B. These limitations were clearly observed in the column experiments using actual hydrothermally altered rock producing alkaline leachate. The migration of both As and B was only temporarily retarded by the adsorption layer. In addition, the persistent alkaline pH of the leachate not only reduced adsorption but also destabilized both the geogenic and adsorbed As in the natural adsorbent. None the less, natural geologic materials like partly-weathered volcanic ashes that have high amorphous Al and Fe

contents are effective adsorbents of As especially in systems with circumneutral pH and under slightly to moderately oxidizing conditions.

Acknowledgment

A part of this study was financially supported by the Japan Society for the Promotion of Science (JSPS) grant-in-aid for scientific research. The authors also wish to thank the anonymous reviewers for their valuable inputs to this paper.

References

Anawar, H.M., Akai, J., Sakugawa, H., 2004. Mobilization of arsenic from subsurface sediments by effect of bicarbonate ions in groundwater. Chemosphere 54(6), 753-62.

Bethke, C.M., 2007. Geochemical and Biogeochemical Reaction Modelling, 2nd edition, Cambridge University Press, New York.

Chakraborty, A.K., Saha, K.C., 1987. Arsenical dermatosis from tubewell water in West Bengal. Indian J. Med. Res. 85: 326-334.

Chen, C.J., Chen, C.W., Wu, M.M., Kuo, T.L., 1992. Cancer potential in liver, lung, bladder and kidney due to ingested inorganic arsenic in drinking water. Br. J. Cancer 66(5), 888-892.

Chen, Z., Kim, K.W., Zhu, Y.G., McLauren, R., Liu, F., He, J.Z., 2006. Adsorption ($As^{III,V}$) and oxidation (As^{III}) of arsenic by pedogenic Fe-Mn nodules. Geoderma 136, 566-572.

Du Laing, G., Rinklebe, J., Vandecasteele, B., Meers, E., Tack, F.M.G., 2009. Trace metal behaviour in estuarine and riverine floodplain soils and sediments: A review. Sci. Total Environ. 407, 3972-3985.

Dzombak, D.A., Morel, F.M.M., 1990. Surface Complexation Modeling: Hydrous Ferric Oxide, John Wiley and Sons, New York.

Fail, P.A., Chapin, R.E., Price, C.J., Heindel, J.J., 1998. General, reproductive, developmental, and endocrine toxicity of boronated compounds. Reproductive Toxicology Review, 12(1), 1-18.

Frohne, T., Rinklebe, J., Diaz-Bone, R.A., Du Laing, G., 2011. Controlled variation of redox conditions in a floodplain soil: Impact on metal mobilization and biomethylation of arsenic and antimony. Geoderma 160, 414-424.

Igarashi, T., Sasaki, R., Tabelin, C.B., 2013. Chemical forms of arsenic and selenium leached from mudstones. Procedia Earth and Planetary Science 6, 105-113.

Jacques, D., Šimůnek, J., Mallants, D., van Genuchten, M. Th., 2008. Modelling coupled water flow, solute transport and geochemical reactions affecting heavy metal migration in a podzol soil. Geoderma 145, 449-461.

Katsumi, T., Benson, C.H., Foose, G.J., Kamon, M., 2001. Performance-based design of landfill liners. Engineering Geology 60, 139-148.

Lundgren, T., Soderblom, R., 1985. Clay barriers – a not fully examined possibility. Engineering Geology 21, 201-208.

Manaka, M., 2006. Amount of amorphous materials in relationship to arsenic, antimony, and bismuth concentrations in brown forest soil. Geoderma 136, 75-86.

Masscheleyn, P.H., DeLaune, R., William, H.P., 1991. Effect of redox potential and pH on arsenic speciation and solubility in a contaminated soil. Environ. Sci. Technol. 25, 1414-1419.

Meng, X., Bang, S., Korfiatis, G.P., 2000. Effects of silicate, sulfate, and carbonate on arsenic removal by ferric chloride. Water Res. 34, 1255-1261.

Mitsunobu, S., Harada, T., Takahashi, Y., 2006. Comparison of antimony behaviour with that of arsenic under various soil redox conditions. Environ. Sci. Technol. 40, 7270-7276.

McKeague, J.A., Day, J.H., 1965. Dithionite- and oxalate-extractable Fe and Al as aids in differentiating various classes of soils. Can. J. Soil Sci. 46, 13-22.

Mohan, D., Pittman, C.U., 2007. Arsenic removal from water/wastewater using adsorbents: A critical review. Journal of Hazardous Materials 142, 1 – 53.

Nickson, R.T., McArthur, K.M., Ravenscroft, J.M., Burgess, W.G., Ahmed, K.M., 2000. Mechanism of arsenic release to groundwater, Bangladesh and West Bengal. Applied Geochemistry 15, 403-413.

Ogata, A., and Banks, R.B., 1961. A solution of the differential equation of longitudinal dispersion in porous media. U.S. Geol. Surv. Prof. Paper 411-A.

Perkins, P.V., 1995. The consideration of soil boron adsorption and soil solution boron concentration as affected by moisture content. Geoderma 66, 99-111.

Pirajno, F., 2009. Hydrothermal Processes and Mineral Systems. Springer Science, The Netherlands.

Šimůnek, J., Šejna, M., Saito, H., Sakai, M., van Genuchten, M. Th., 2008. The HYDRUS-1D

Software Package for Simulating the Movement of Water, Heat, and Multiple Solutes in Variably Saturated Media, Version 4.08, HYDRUS Software Series 3, Department of Environmental Sciences, University of California Riverside, Riverside, California, USA.

Tabelin, C.B., Igarashi, T., 2009. Mechanisms of arsenic and lead release from hydrothermally altered rock. Journal of Hazardous Materials 169, 980–990.

Tabelin, C.B., Igarashi, T., Takahashi, R., 2012a.The roles of pyrite and calcite in the mobilization of arsenic and lead from hydrothermally altered rocks excavated in Hokkaido, Japan. Journal of Geochemical Exploration 119, 17-31.

Tabelin, C.B., Igarashi, T., Takahashi., R., 2012b. Mobilization and speciation of arsenic from altered rock in laboratory column experiments under ambient conditions. Applied Geochemistry 27, 326-342.

Tabelin, C.B., Igarashi, T., Yoneda, T., 2012c. Mobilization and speciation of arsenic from hydrothermally altered rock containing calcite and pyrite under anoxic conditions. Applied Geochemistry 27, 2300-2314.

Tabelin, C.B., Basri, A.H.M., Igarashi, T., Yoneda, T., 2012d. Removal of arsenic, boron and selenium from excavated rocks by consecutive washing. Water, Air, & Soil Pollution 223, 4153-4167.

Tamm, O., 1922. Eine method zur Bestimmung de anorbanischen Komponente des Gelko mLexes in Boden. Madd. Fran Stat. Skogs. Stockholm 19, 387-404.

Tatsuhara, T., Arima, T., Igarashi, T., Tabelin, C.B., 2012. Combined neutralization-adsorption system for the disposal of hydrothermally altered excavated rock producing acidic leachate with hazardous pollutants. Engineering Geology, 139-140, 76-84.

Wijeyesekera, D.C., O'Connor, K., Salmon, D.E., 2001. Design and performance of a compacted clay barrier through a landfill. Engineering Geology 60, 295-305.

Xu, Y., Jiang, J.Q., 2008. Technologies for boron removal. Ind. Eng. Chem. Res. 47, 16-24.

Figure Captions

FIGURE 1 Schematic diagram of the columns with and without an adsorption layer.

FIGURE 2 Leaching concentration of As vs pH in samples A-1 and A-2.

FIGURE 3 Effects of pH on the leaching concentrations of Fe and Al from A-1 and A-2; (a) Fe concentration change with pH, and (b) Al concentration change with pH.

FIGURE 4 Adsorption characteristics of As onto natural geologic materials fitted with linear, Freundlich and Langmuir isotherms; (a) A-1, (b) A-2, (c) S-1, and (d) S-5.

FIGURE 5 Adsorption characteristics of B onto natural geologic materials fitted with linear, Freundlich and Langmuir isotherms; (a) A-1, (b) A-2, (c) S-1, and (d) S-5.

FIGURE 6 Correlations of the adsorption capacity (q_{max}) of As and K_D of B with the amorphous Al and Fe contents of several natural geologic materials; (a) q_{max} vs amorphous Al and Fe content, and (b) K_D vs amorphous Al and Fe content.

FIGURE 7 Zeta potential of sample A-1 vs pH.

FIGURE 8 Effects of the adsorption layer on the properties of the effluent with time; (a) pH change with time, (b) Eh change with time, (c) EC change with time, (d) As concentration change with time, (e) B concentration change with time, (f) Ca^{2+} concentration change with time, (g) Na^{+} concentration change with time, and (h) SO_4^{2-} concentration change with time.

FIGURE 9 Simulation of As and B migration in the column experiments using the extended advection-dispersion equation with retardation; (a) As migration in case R+A2, and (b) B migration in case R+A2.

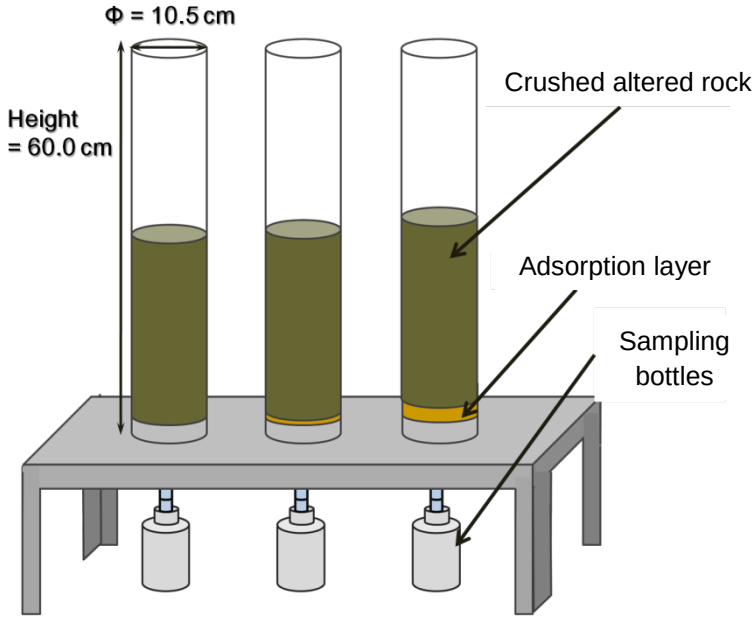

Figure 1

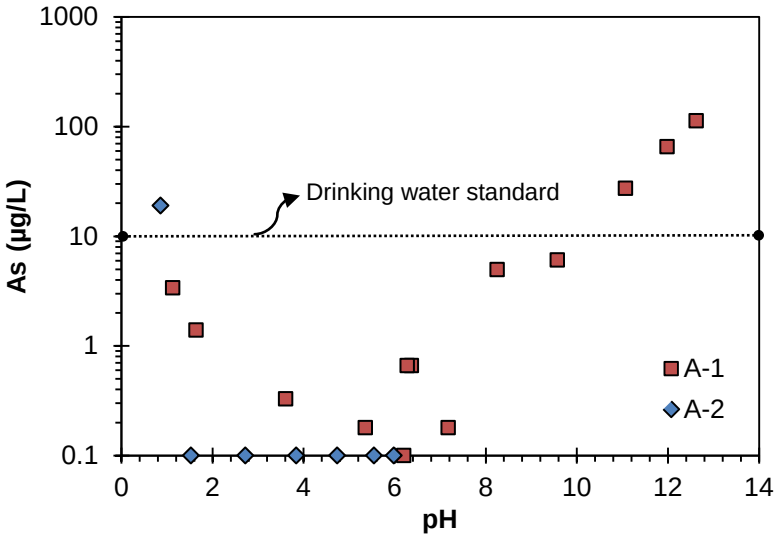

Figure 2

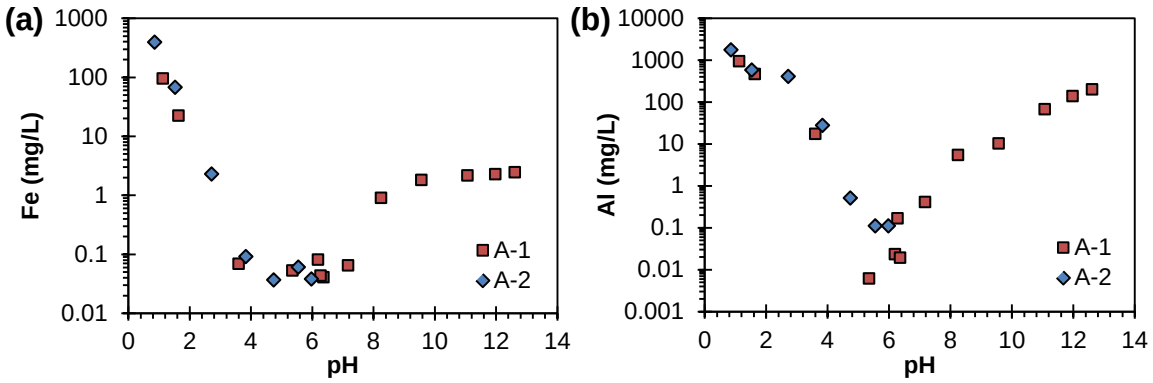

Figure 3

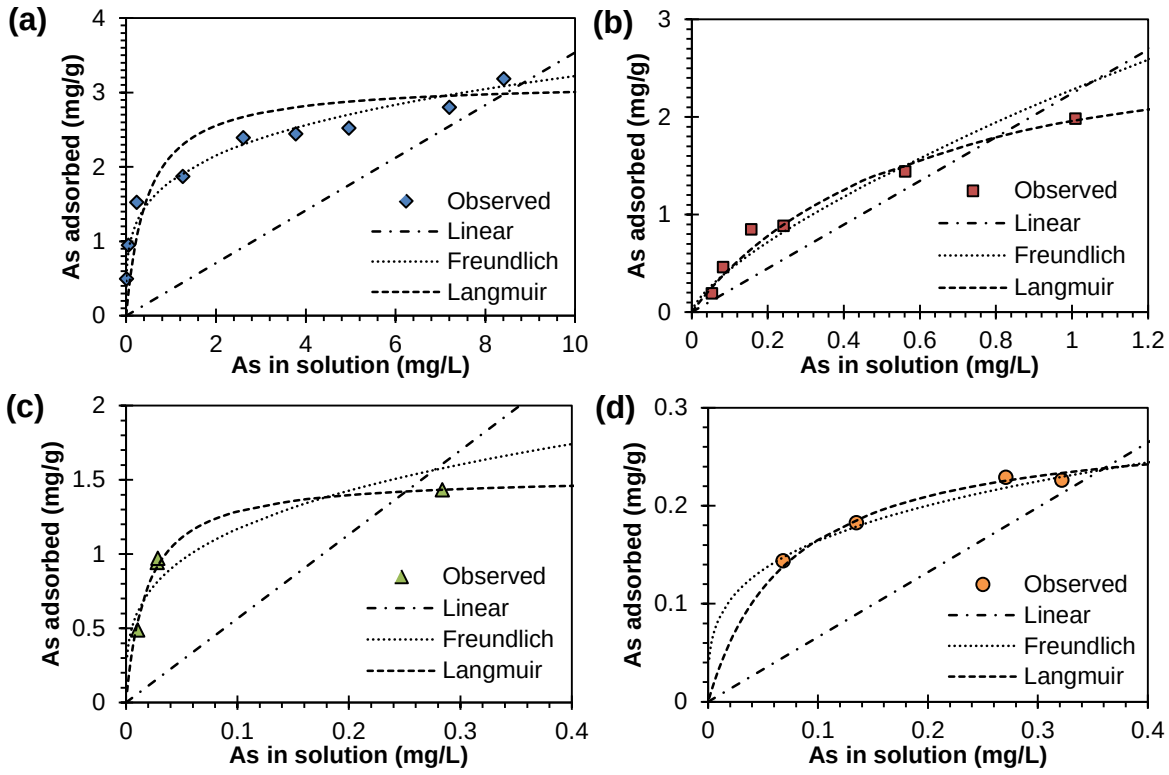

Figure 4

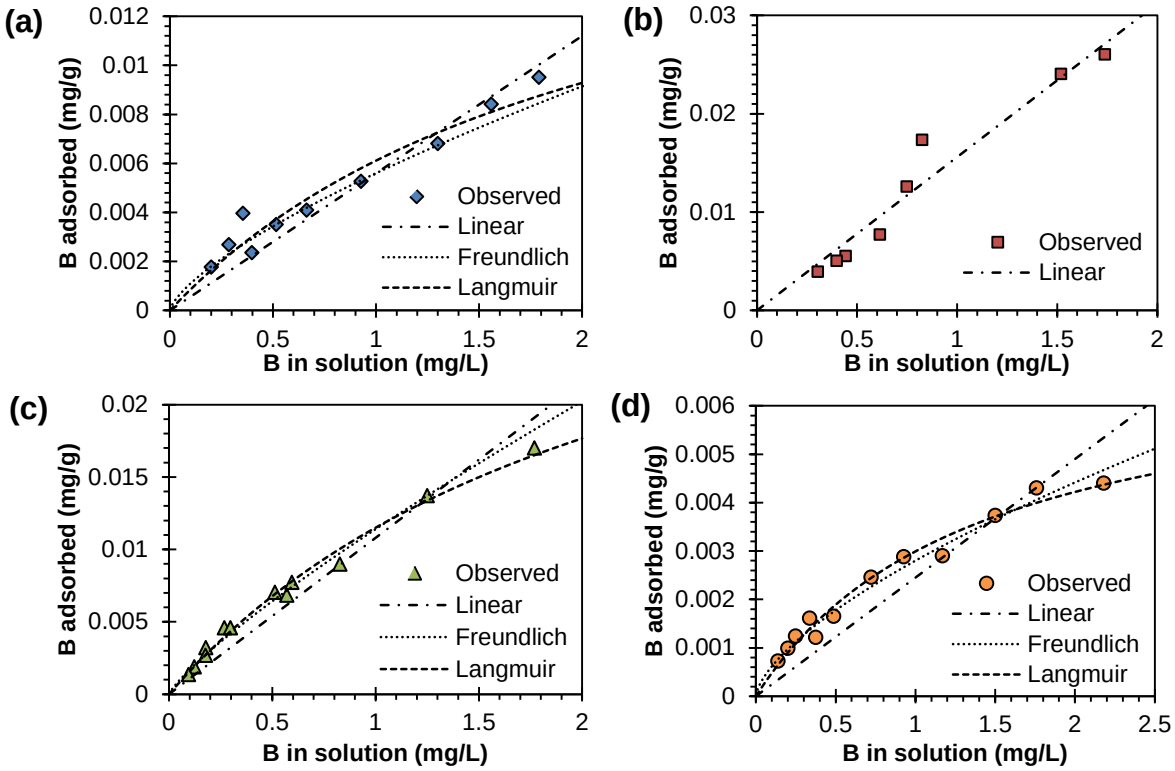

Figure 5

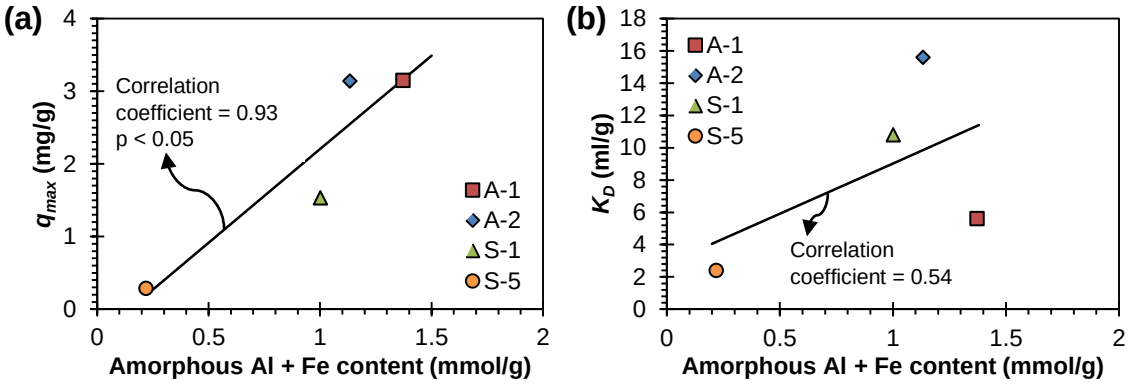

Figure 6

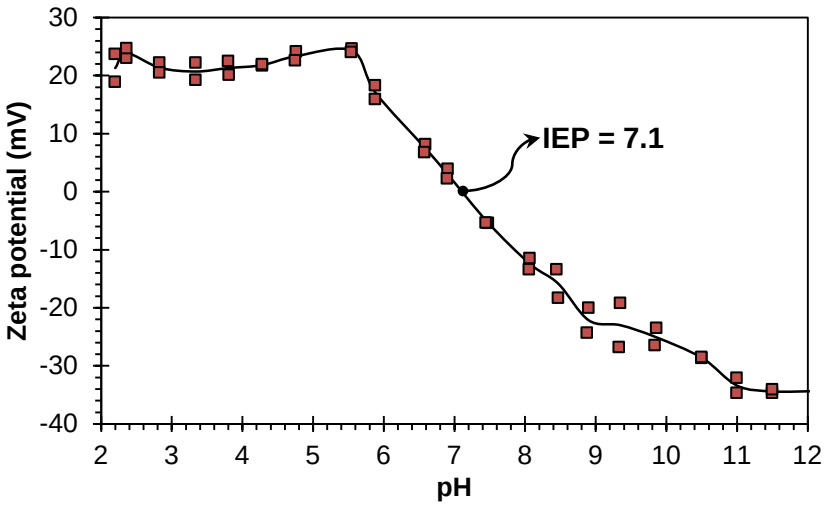
Zeta potential (mV)
30
20
10
0
-10
-20
-30
-40
2
3
4
5
6
7
8
9
10
11
12
pH
IEP = 7.1

Figure 7

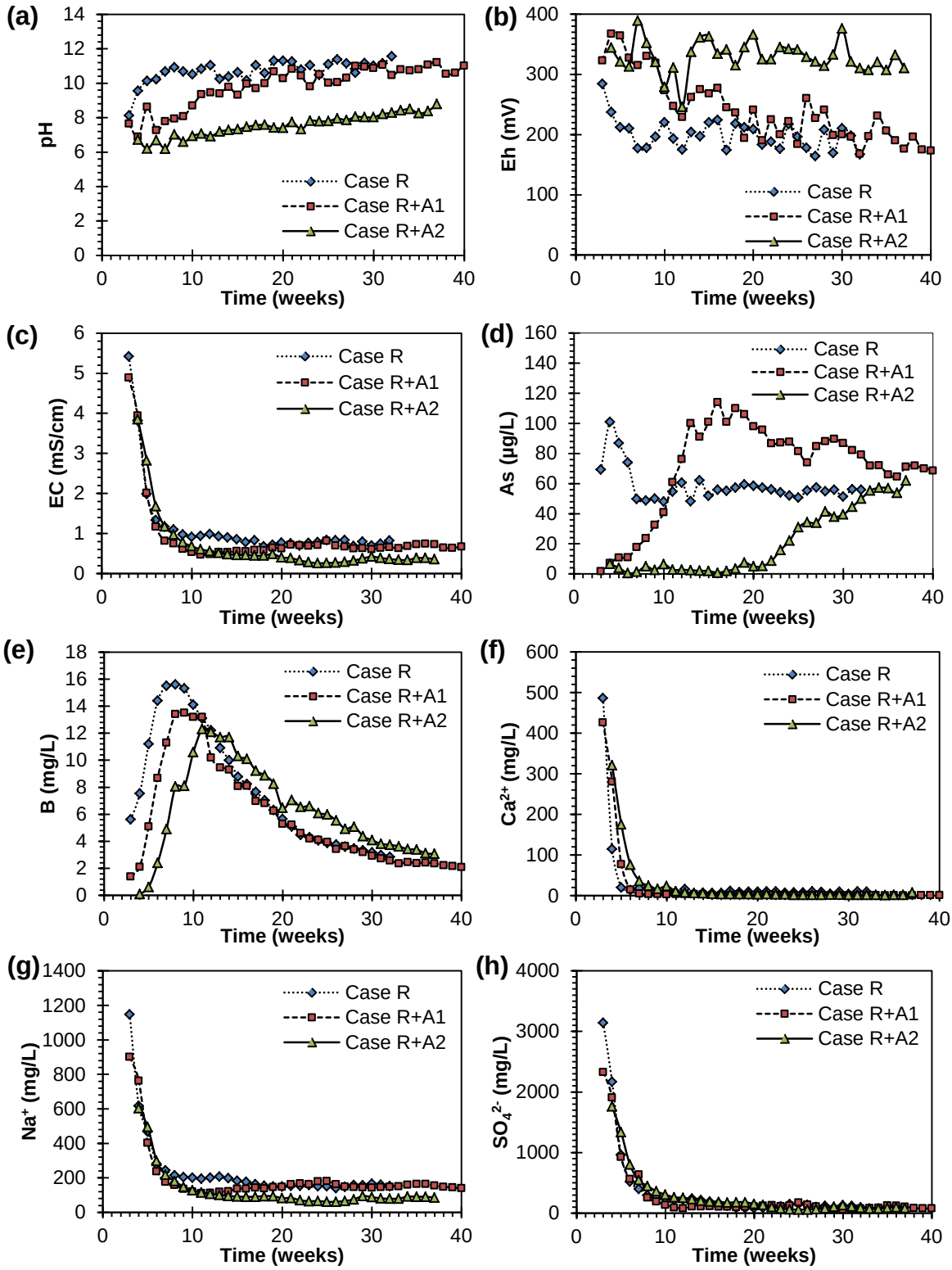
(a)
pH
Time (weeks)
Case R
Case R+A1
Case R+A2
(b)
Eh (mV)
Time (weeks)
Case R
Case R+A1
Case R+A2
(c)
EC (mS/cm)
Time (weeks)
Case R
Case R+A1
Case R+A2
(d)
As (µg/L)
Time (weeks)
Case R
Case R+A1
Case R+A2
(e)
B (mg/L)
Time (weeks)
Case R
Case R+A1
Case R+A2
(f)
Ca2+ (mg/L)
Time (weeks)
Case R
Case R+A1
Case R+A2
(g)
Na+ (mg/L)
Time (weeks)
Case R
Case R+A1
Case R+A2
(h)
SO4 2- (mg/L)
Time (weeks)
Case R
Case R+A1
Case R+A2

Figure 8

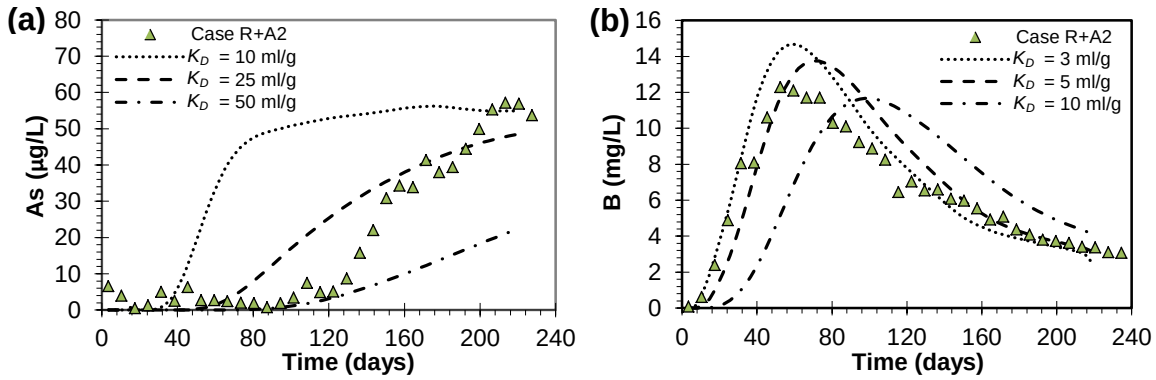
(a)
Case R+A2
K_D = 10 ml/g
K_D = 25 ml/g
K_D = 50 ml/g
As (µg/L)
Time (days)
(b)
Case R+A2
K_D = 3 ml/g
K_D = 5 ml/g
K_D = 10 ml/g
B (mg/L)
Time (days)

Figure 9

Table 1. Description of the natural geologic materials and their sampling locations

Sample	Description	Category
T-1	Pumiceous tuff	Loamy sand
T-2	Pumiceous tuff	Loamy sand
T-3	Pumiceous tuff	Loamy sand
A-1	Partly-weathered volcanic ash	Loamy sand
A-2	Partly-weathered volcanic ash	Clay loam
S-1	Coastal marine sediment	Sandy loam
S-2	Coastal marine sediment	Loamy sand
S-3	Coastal marine sediment	Conglomeratic sandy loam
S-4	Coastal marine sediment	Conglomeratic sandy loam
S-5	Coastal marine sediment	Sandy loam
S-6	Coastal marine sediment	Loamy sand

Table 2. List of column experimental conditions

Column notation	Infiltration rate (mm/week)	Altered rock layer			Adsorption layer			
		Thickness (mm)	Bulk density (g/cm^3)	Porosity (%)	Adsorbent used	Thickness (mm)	Bulk density (g/cm^3)	Porosity (%)
Case R	34.5	300	1.28	53.3	-	-	-	-
Case R+A1	34.5	300	1.28	53.3	A-1	10	0.72	74.9
Case R+A2	34.5	300	1.28	53.3	A-1	30	0.72	74.9

Table 3. Parameters used in the analytical model

Number of layers	1
Thickness of layer	3 cm
Particle density	2.87 g/cm^3
Bulk density	1.28 g/cm^3
Porosity	0.748
Flow conditions	Unsaturated-steady state
Linear velocity	0.682 cm/day
Volumetric water content	0.582 cm^3/cm^3
Dispersivity (α)	0.4 cm
Initial and boundary conditions	
$t \leq 0, x \geq 0, C = 0$	
$t > 0, x = 0, C = C_0$	
$x = \infty, C = 0$	
Solute transport boundary conditions	
Upper boundary	Step function based on As and B concentrations in case R
Lower Boundary	$C = 0$ ($x \rightarrow \infty$)

Table 4. Physical and hydrological properties of the natural geologic materials

Sample	Wet density (g/cm^3)	Dry density (g/cm^3)	Particle density (g/cm^3)	Particle size distribution (%)				Hydraulic conductivity (m/s)
				Gravel 2 – 75 mm	Sand 0.075 – 2 mm	Silt 0.005 – 0.075 mm	Clay <0.005 mm	
T-1	1.54	1.25	2.50	0.0	79.6	16.3	4.1	4.17×10^{-6}
T-2	1.67	1.26	2.43	17.4	62.2	16.8	3.6	2.43×10^{-6}
T-3	1.25	1.11	2.41	3.5	72.5	20.4	3.6	1.85×10^{-5}
A-1	1.41	1.10	2.87	0.0	70.9	22.1	7.0	4.66×10^{-6}
A-2	-	-	2.70	0.2	28.2	41.0	30.4	1.61×10^{-6}
S-1	1.42	0.94	2.79	0.9	58.6	24.1	16.4	9.98×10^{-6}
S-2	1.70	1.30	2.73	0.0	87.5	9.5	3.0	2.32×10^{-5}
S-3	1.70	1.25	2.72	6.7	71.0	14.4	7.9	1.38×10^{-6}
S-4	1.59	1.19	2.73	14.8	68.5	11.0	5.7	6.65×10^{-6}
S-5	1.47	1.09	2.70	0.2	59.9	27.2	12.7	7.65×10^{-6}
S-6	1.70	1.43	2.74	1.4	83.5	10.4	4.7	2.10×10^{-6}

*-: Not measured

Table 5. Chemical composition of the natural geologic materials

Sample	SiO_2 wt%	TiO_2 wt%	Al_2O_3 wt%	Fe_2O_3 wt%	MnO wt%	MgO wt%	CaO wt%	Na_2O wt%	K_2O wt%	P_2O_5 wt%	S wt%	As (mg/kg)
T-1	58.5	0.27	12.4	2.79	0.06	0.73	1.30	0.92	2.67	0.001	0.0001	2.6
T-2	65.9	0.16	9.32	1.74	0.03	0.42	1.18	1.20	3.39	0.001	0.0001	4.03
T-3	69.9	0.15	9.53	1.67	0.04	0.24	1.22	1.48	3.34	0.002	0.0002	1.74
A-1	51.2	0.96	20.4	10.5	0.18	3.42	3.86	1.38	1.13	0.16	0.01	1.18
A-2	51.3	0.95	21.7	9.02	0.20	2.33	0.95	1.21	2.01	0.23	0.11	2.05
S-1	52.6	0.95	24.0	10.3	0.21	1.70	3.30	0.24	1.09	0.17	0.05	7.89
S-2	61.6	0.73	14.2	7.46	0.13	3.42	4.58	0.94	2.32	0.04	0.0002	2.05
S-3	58.8	0.94	16.4	7.92	0.11	1.69	3.26	0.24	1.27	0.01	0.0002	1.97
S-4	56.8	0.80	18.5	8.23	0.17	1.31	2.69	0.65	1.39	0.04	0.0002	1.97
S-5	55.7	0.77	21.1	7.49	0.10	1.08	0.72	0.23	1.30	0.001	0.0005	8.05
S-6	58.4	1.10	17.1	10.6	0.17	1.76	3.52	0.42	1.20	0.08	0.02	1.97

Table 6. Mineralogical composition of the natural geologic materials determined using XRD

Material	Qtz	Ab	Chl	An	Hal
T-1	+++	++			
T-2	+++	++			
T-3	+++	++		+	
A-1	+++	++	+		
A-2	+++		+	++	
S-1	+++	++			
S-2	+++	++			
S-3	+++	++			
S-4	+++	++			
S-5	+++	++			+
S-6	+++	++		+	

+++: Major; ++: Moderate; +: Minor.
Qtz: Quartz; Ab: Albite; Chl: Chlorite; An: Anorthite; Hal: Halloysite

*Note: In samples with little or no volcanic glass (*e.g.*, coastal sediments), major, moderate, minor and trace roughly represent >30%, 10-30% and 2-10%, respectively.

Table 7. Amorphous Al and Fe contents of the natural geologic materials

Sample	Al (mg/g)	Fe (mg/g)	Al+Fe (mmol/g)
T-1	0.45	0.18	0.02
T-2	0.30	0.46	0.02
T-3	0.19	0.11	0.01
A-1	32.1	10.2	1.37
A-2	24.0	13.6	1.13
S-1	22.1	9.16	1.10
S-2	1.44	0.74	0.07
S-3	2.50	2.86	0.14
S-4	1.86	3.03	0.12
S-5	3.37	5.27	0.21
S-6	1.29	1.13	0.07

Table 8. Linear, Freundlich and Langmuir isotherm constants for As

Sample	Linear (equation (2))		Freundlich (equation (3))			Langmuir (equation (4))		
	K_D (ml/g)	R	K_f (ml/g)	n	R	L	q_{max} (mg/g)	R
A-1	354	0.86	1,810	0.25	0.98	2.15	3.15	0.99
A-2	2,240	0.86	2,280	0.718	0.95	1.65	3.14	0.93
S-1	5,659	0.51	2,260	0.287	0.90	53.2	1.53	0.99
S-5	661	0.62	317	0.286	0.99	13.6	0.287	0.99

Table 9. Linear, Freundlich and Langmuir isotherm constants for B

Sample	Linear (equation (2))		Freundlich (equation (3))			Langmuir (equation (4))		
	K_D (ml/g)	R	K_f (ml/g)	n	R	L	q_{max} (mg/g)	R
A-1	5.6	0.95	5.9	0.707	0.96	0.456	0.019	0.79
A-2	15.6	0.97	-	-	-	-	-	-
S-1	10.8	0.97	1.1	0.828	0.99	0.432	0.038	0.90
S-5	2.4	0.90	2.8	0.657	0.99	0.717	0.007	0.95